AUTHOR QUERIES

AUTHOR PLEASE ANSWER ALL QUERIES

AQ1: Please confirm or add details for any funding or financial support for the research of this article.

AQ2: It was indicated that research for this article involved either human subjects or animals. Please provide approval obtained from a relevant review board (or local/regional equivalent).

AQ3: Please provide the department name for Orsi Academy.

AQ4: Please provide the postal code for Verona University Hospital, Verona, Italy.

AQ5: Please provide the page range for Reference [20].

Preclinical Validation of a Semi-Autonomous Robot for Transperineal Prostate Biopsy

Bogdan Maris©, Maria-Camilla Fiazza, *Member, IEEE*, Michela De Piccoli, Chiara Tenga, Luigi Palladino©, Stefano Puliatti, Andrea Iseppi, Riccardo Ferrari, Adele Piro, Luca Reggiani Bonetti, Guido Ligabue, Alessandro Tafuri, Salvatore Micali, and Paolo Fiorini©, *Life Fellow, IEEE*

Abstract—Prostate biopsy is a manual procedure carried out mostly under ultrasound (US) guidance to confirm the presence of cancer. The standard biopsy is random and includes at least 12 insertions; targeted biopsy makes use of dedicated hardware and software, but is still performed manually. We present here the pre-clinical validation of PROST, a robot primarily designed to automate targeted transperineal biopsy. The overall validation of the system was performed on cadavers, while some features, such as image segmentation, were tested on human tissue. PROST is designed to minimize human error by introducing some autonomy in the execution of key steps of the procedure, i.e., target selection, image fusion and needle positioning. The protocol was approved by the ethics committee; 10 cadavers were included in the study. We envision that PROST has the potential to increase the detection of clinically significant prostate cancer, to simplify the procedure, to reduce human errors and to shorten training time. The use of a robot for the biopsy of the prostate will create the possibility to include also a treatment, such as focal ablation, to be delivered through the same system.

Index Terms—Surgical robotics, medical robotics, prostate biopsy, autonomous robot, translational research.

I. INTRODUCTION

NEEDLE biopsy is currently the most reliable and widely used technique to confirm the suspicion of prostate cancer (PCa), the second most common cancer worldwide and the cancer most common in men [1]. Biopsy cores can provide information on the cancer's aggressiveness (grade) and contribute to assessing its stage [2]. The majority of biopsy procedures are performed manually, with freehand technique and with the aid of a transrectal ultrasound probe to facilitate anatomical navigation and aiming (TRUS).

The gold standard for PCa detection remains systematic transrectal biopsy (12 or more cores). Decades of data and the disadvantages being well understood make it the reliable term of comparison for all innovations in PCa detection. MRI/US fusion targeted biopsy—in which the physician directly targets suspect lesions previously identified via MRI—has shown detection rates from comparable to better than systematic TRUS biopsy, even with a much-reduced number of cores (2 to 4) [3], [4].

Machines play a critical role in assisting the physician: first with determining the location of suspect lesions and then with accurately reaching them. Fusion MRI/US guidance systems facilitate the mental overlap between pre-operative MR imaging and intra-operative US imaging. As a result, the targets are more accurately localized in the US image space. Commercial examples include *Uronav* (Philips Medical Systems, Netherlands), *Real-Time Virtual Sonography* (Hitachi, Tokyo, Japan) and *Virtual Navigator* (Esaote, Genoa, Italy). Some, such as *BK Fusion* (Analogic, Peabody, MA, USA) expand on previous proprietary hardware, whereas others, such as *Koelis Trinity* (Koelis, Meylan, France) have developed an extensive suit of proprietary software, including patented methods for image fusion [5].

A second family of machine-mediated improvements consists in helping the physician accurately *reach* the target locations, by registering the image space with the physical space. Research prototypes (e.g., [6]) or commercial systems such as *Artemis* (Eigen, Grass Valley, CA, USA) and *iSR'obot MonaLisa* (Biobot Surgical LTD, Singapore) use a robotic arm to orient a guide in the direction of the target. The physician need only slide the biopsy needle along the guide.

The traditional access path for prostate biopsies is transrectal. Transperineal access has been growing in prominence thanks to a lower risk of complications (especially fever and rectal bleeding) in the face of comparable diagnostic

Fig. 1. Artist rendering of the prostate biopsy positioning head (PROST) as a component of a larger robotic system, that may be used also for other procedures. For the experiments described in this paper, the robotic head was mounted on a wheeled cart.
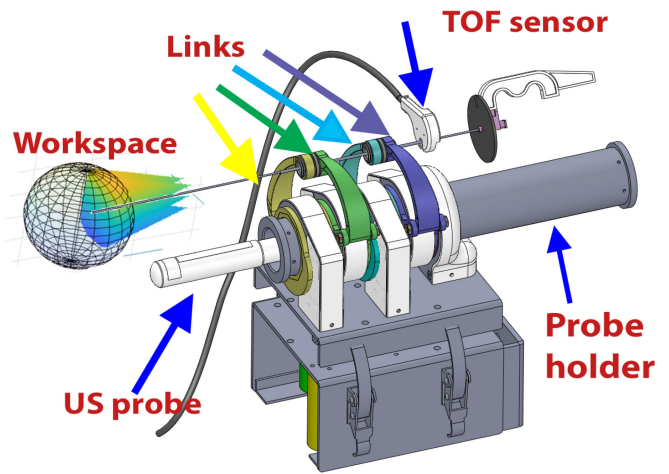

Fig. 2. CAD of the PROST robot showing the workspace and the time of flight (TOF) sensor that measures the depth of the needle insertion.

efficiency [7]. An important consideration is the growing risk of antibiotic-resistant infection as a sequela of transrectal biopsy. Concerns about fluoroquinolone resistance and multiresistant rectal flora are addressed with patient-specific antibiotic prophylaxis, determined after a rectal swab. The risk of infection from the perineal access, on the other hand, can be addressed with a single dose of cephalosporines [8].

There are indications of a superior sensitivity in detecting anterior cancers when approaching from the perineum [9]. There have also been indications that, like TRUS, transperineal biopsy can safely be performed in local anesthesia [10]. The standard practice has been general anaesthesia, a significant disadvantage with respect to TRUS.

To benefit maximally from the perineal access path, one could try extracting multiple cores from the same entry point, thereby minimizing surgical trauma. In freehand procedures, great skill would be required on the physician's side to implement this improvement, whereas robot assistance could render it accessible in a straightforward manner [11].

Both access paths are represented in commercial systems for prostate biopsy. For example, *Koelis Trinity* and *MonaLisa* have been developed for the transperineal approach, whereas [6] and [12] target transrectal procedures. *Artemis* supports both. A review of technology for assisted prostate biopsy can be found in [13].

The PROST robotic head is part of a larger medical robotic system (Fig. 1) to enable effective robot-assisted biopsies. Its goal is improving detection rates of PCa by leveraging the strong points of machines in every component of the procedure. PROST is designed for ultrasound-guided transperineal biopsies also in outpatient settings. It offers MRI/US fusion, needle alignment and cognitive support for target selection and entry point planning. The conical workspace of the positioning robot enables sampling any point on the prostate using at most two pivot (entry) points on the perineum (Fig. 2). Additional points may be required if special clinical considerations result in large exclusion areas that forbid many needle trajectories.

All existing prostate biopsy systems support some automatic functions. PROST's development is driven by the belief that autonomy improves accessibility and empowers physicians by enabling new functionalities. For example, fusion systems that support biopsy planning do not adapt the plan to intra-operative changes in the prostate, even when the prostate's position is updated dynamically (e.g., *Koelis*). The accuracy of targeted biopsy is negatively affected by the lack of compensation in the plan. This is often due to a reliance on the physician to manually segment the prostate at the time of the initial image fusion. Even though expert users can complete the task in few minutes if the interface is intuitive, the time scale is not compatible with intra-operative replanning. It is not feasible to halt the procedure for few minutes to receive help from the physician in updating the reference segmentation. Autonomous semantic segmentation of the prostate based on convolutional neural networks (CNNs), on the other hand, would enable replanning and prevent a loss of accuracy.

Improving the accessibility of high-quality prostate biopsy is a key desired impact of PROST's development, and is pursued in multiple ways: by explicitly targeting outpatient settings, by successfully helping physicians bridge the experience gap quickly, and by automating steps so as to lower the overall duration of the procedure.

II. Experimental Validation Strategy

We have previously described the laboratory validation of a PROST prototype in [14]. The clinical objective is sampling lesions in regions where cancer is suspected, from volumes approximately ellipsoid or spheroid in shape, with axes greater than 5-7 mm. Extensive laboratory testing was carried out on phantoms.

At first, a 3D-printed rigid geometric structure immersed in a US-transparent silicone shell was used to evaluate the device's positioning accuracy. The structure links several 2-mm targets, which are much smaller than the lesions typically targeted in biopsy procedures, as only those larger than 5-7 mm in diameter are considered clinically significant [2]. The results—a positioning accuracy of 1.30 ± 0.44 mm— provided a baseline validation for the mechanical apparatus (kinematics and control), calibration and integration with real-time US data, and also the adequacy of sensors.
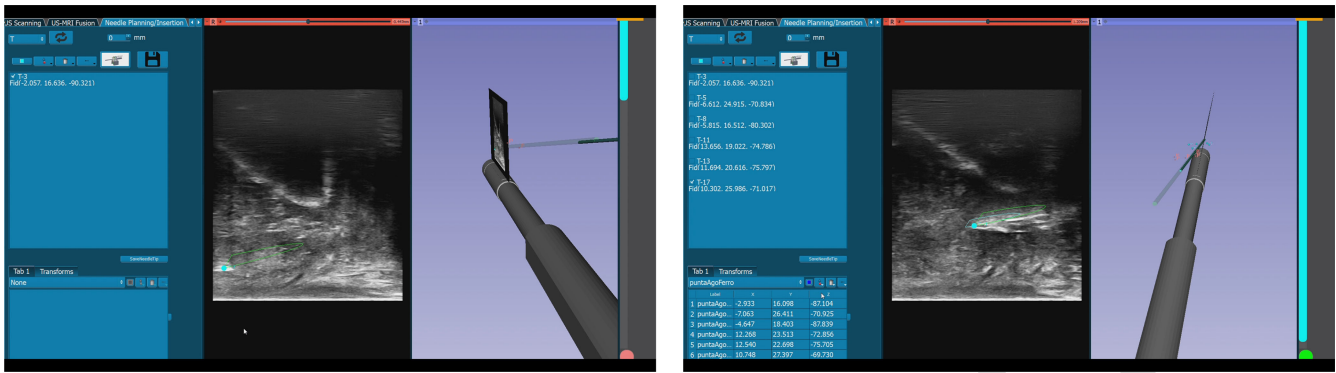
Fig. 3. Graphical user interface (GUI). As compared with our previous phantom tests [14], in the cadaver tests the visibility of the prostate in the 2D US image is difficult and the 3D visualization includes only the US probe, the needle trajectory and position, and the projection of the 2D US image. **Left:** once the target is defined, the GUI shows a virtual path in 2D and 3D (green). **Right:** 6 target seeds and 6 reference seeds were defined (the list of points is on the left of the screen); the needle is inserted toward the last target and a blue path shows the actual trajectory; the progress bar shows the distance to the target, represented by a green circle.

Secondly, commercial anatomical phantoms (CIRS 070 and CIRS 053, Computerized Imaging Reference Systems, Inc., Norfolk, Virginia, USA), modeling the prostate and surrounding structures, were used to extend the validation to a realistic anatomy, albeit with simplified signals. This step allowed testing the overall architecture, the fusion of intra-operative ultrasound imaging and a pre-operative MR scan, and the integration with segmentation algorithms. Lesions were 10 mm in diameter, in the clinical range. The results (accuracy of 1.54 ± 0.34 mm) are comparable to the previous case and remained well within the margins suitable for clinical use. With these tests, PROST met the benchmark for Technology Readiness Level 4 (TRL 4).

The next step is transitioning to the much harder case of realistic anatomical signals, assessing PROST's performance with the complex and noisy signals generated by real-time imaging of human tissues in a realistic environment (TRL 6). In this paper, therefore, we build on the previous mechanical results and focus on two further aspects of PROST's validation: segmentation of the anatomical scene on patient data and testing guided needle insertion on cadavers.

Testing on human cadavers is preferable to animal testing whenever the system targets procedures and anatomical areas which may differ significantly in animals. In our case, although the general topology of the prostate area in pigs is comparable to that in humans [15], reachability of the prostate, access paths, organ size and distances are different and can significantly affect mechanical design.

Biopsying the prostate post-mortem in situ can, however, also introduce new challenges. The physical properties of the organ's tissues can change significantly from in-vivo conditions. Particularly relevant are changes in elasticity and firmness. These changes are partly due to the process of freezing and thawing of the specimen, and partly due to the absence of blood flow, as the prostate is a highly vascularized gland. Furthermore, ultrasound imaging of cadaver tissues is negatively affected by tissue dehydration and by the lack of a full bladder, used to provide a landmark and orient in the anatomy. Overall, the cadaver testing conditions are different than regular clinical conditions. Therefore, only part of the complete robotic setup can be tested. We explain these conditions further in the following sections and we describe the challenges we faced.

The rest of this paper is organized as follows: Section III presents an overview of PROST's hardware structure and of key elements of the workflow. Section III-C introduces the segmentation strategy and its performance. Sections IV and V describe the cadaver experiments and discuss the results. Section VI concludes by summarizing the key results and describing our plans for future developments of the system.

III. THE PROST ROBOTIC SYSTEM

A. Positioning Robot

An in-depth description of PROST's mechanics was introduced in [14], so we report here only the main features. PROST is composed of two two-joint arms that move along parallel planes (Fig. 2). The arms orient a cannula and the biopsy needle passes through the cannula to reach the target.

The robot uses 5 motors and has 5 degrees of freedom (DOFs): 2 DOFs for reaching the entry position, 2 DOFs for needle orientation and 1 DOF for the US probe. The motors are located in a box under the links. The box is detachable for sterilization purposes.

PROST is able to keep a fixed entry point for a set of selected targets. Computation of the entry point is optimized via software so that the movement is minimal. The target and the entry points give the orientation of the needle; the software will compute the inverse kinematic and will move the links accordingly.

Through intensive calibration tests, we measured a calibration accuracy at the needle tip of less than 1 mm (see [14]).

PROST integrates a bi-planar US probe compatible with Ultrasonix US system (BK Medical, Peabody, Massachusetts, USA). The US image is calibrated with the robot reference system using the PLUS toolkit [16].

The communication between the robot and the image stream is real-time, using the open-source libraries OpenIGTLink [17]. The user interface (Fig. 3) is based on 3D Slicer modules and was developed in Python. The

image segmentation software (Section III-C) was also written in Python and integrated as a module in 3D Slicer.

B. Level of Autonomy

PROST's goal is to reduce margins for human error in prostate biopsy procedures, wherever machines can improve on human performance. This means providing assistance, both manual and cognitive, with the declared goal of designing for increasing levels of autonomy. The same technology that one uses in an assistive modality of operation, once it matures enough in reliability and can be certified for safety, can be used in an autonomous modality, with a human supervisor.

While the system's autonomous capabilities are under development, for safety reasons we run PROST in assistive mode. The physician bears responsibility for the clinical decisions, including which tasks to delegate to PROST. All high-level decisions can be over-ridden by the physician, who can manually change or fine-tune segmentation, image fusion, registration, trajectories and entry points. The lower-level decisions (such as the operation of the positioning robot), on the other hand, are autonomous. The physician only initiates the positioning task, by approving the choice of target location and the entry point. These operations are carried out by machines in a reliable, quantifiable and consistent manner with greater accuracy and precision than humans, who cannot be expected to oversee such low-level decisions effectively.

For now, PROST makes a *proposal* to the physician, who assesses it–and can approve it, request another proposal or input a value directly, according to his or her clinical judgment. PROST facilitates the biopsy by accurately orienting a standard guide (cannula) for biopsy needles toward the next desired target; the physician then manually inserts the biopsy needle. PROST is compatible with all types of biopsy needles for prostate procedures. Insertion is assisted, in the sense that PROST's GUI monitors the current depth of the needle tip and its estimated distance from the target location. The doctor retains the complete control of the surgical task. Through PROST's graphical user interface (GUI), the insertion is monitored in 2D and 3D (Fig. 3), along with the current distance from the target location. The insertion is manual so that the doctor retains the complete control of the surgical task.

The PROST prototype we describe here operates in assistive mode at autonomy level 2 (Task Autonomy), according to the classification in [18], and at LoA 2 (Task-level autonomy) according to [19]. This level corresponds to degree of autonomy (DoA) 3-5, in the finer classification based on IEC/TR 60601-4-1. Depending on the subtask considered—e.g., entry point selection or MRI/US fusion—PROST can be placed at DoA 3 (Shared Decision), DoA 4 (Decision Support), or DoA 5 (Blended Decision).

PROST is a needle guide system for the perineal access in prostate biopsy; the insertion of the needle is manual and there is no mechanical structure at the skin entry point. The forces exerted on the patient are on the needle. PROST is used only to orient the cannula (Fig. 2) and the free space between the needle guide and the skin is minimal to reduce needle deflection and lateral buckling.

Save for rotating the US probe on its axis, the robot does not interact with the patient's body directly, thus limiting safety concerns. The only contact point is the rectum. The safety issues of autonomous operation can be addressed simply by limiting friction and range of motion: by using sufficient gel around the probe, by placing an upper bound on probe rotation speed and by limiting the angular displacement to the range necessary for the prostate and surrounding tissues to be brought into view.

C. CNNs for Semantic Segmentation

The PROST system includes a software module implementing a dedicated convolutional neural network that we called PROST-Net [20], [21]. This module allows the segmentation of the prostate in US and MRI images for the purpose of image fusion (Fig. 4). The pre-clinical validation of this module is made on patient data obtained after ethical approval. We specify also that the module was not tested on cadaver images, because the US images of ex-vivo prostate tissue differ considerably compared with in-vivo tissue and MRI data of cadavers were not available. Some preliminary results on patient data and phantom images are reported in this section, since this module is still under development.

The PROST-Net architecture derives from Mask R-CNN [22] and U-Net [23], assembling the best of both for the purpose of real-time segmentation of the prostate in US and MRI images (Fig. 4). It takes the detection part from Mask R-CNN to find a region of interest (ROI), which is a bounding box that perfectly fits the prostate shape. This allows the segmentation sub-network to contour the prostate regardless of the scanning plane. In our implementation, the ROI extracted by the region proposal network (Fig. 4) is given as input to the second part of the network which exploits a recurrent architecture like U-Net, but with a reduced amount of max-pooling and upconvolution steps and with application of residual blocks and dropout layers. This approach permitted to exploit the strong part of a regional network but also the typical aspects of employing a "U-Net like" architecture which works better on medical images, where typically the amount of data is limited.

The method was first tested on prostate phantoms CIRS 070 and CIRS 053 (Computerized Imaging Reference Systems, Inc., Norfolk, Virginia, USA) and subsequently on patient datasets [21].

We firstly tested the method on phantoms. The images were acquired using an Ultrasonix US machine (BK Medical, Peabody, Massachusetts, USA) from two standard synthetic phantoms (CIRS 070 and CIRS 053) containing the prostate with urethra and seminal vesicles, the bladder, and the rectum. The dataset was composed by 2347 axial and 842 sagittal images.

A second phase of experiments involved the use of patients dataset composed of 840 images for training and validation and 664 images for testing. The dataset comprehends both axial and sagittal images recorded with a Hitachi Aloka 70 (Hitachi Healthcare Americas, Twinsburg, USA) and a biplanar probe.The data and the ground truth was obtained with
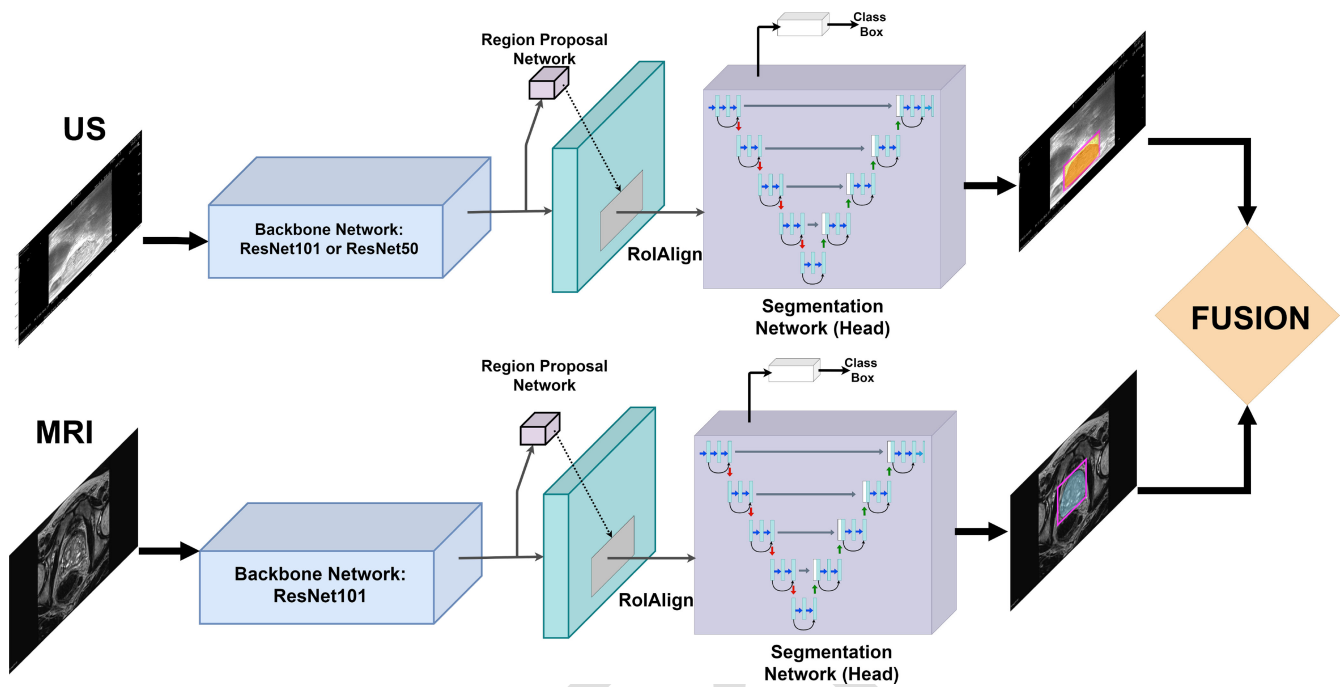
Fig. 4. The PROST-Net architecture to segment the prostate from US and MRI images. The output of the segmentation is used to fuse the two imaging modalities in the reference system of the PROST robot.

the support of the local hospital and with the approval of the ethics committee.

PROST-Net network is initialized with the original COCO dataset training weights [24] to improve performance and significantly reduce the training time, as demonstrated in [25]. We performed a series of epoch training as long as the loss function keeps on decreasing its value. These preliminary training modifies only head layers. By doing this, we freeze all the backbone layers and train only the RPN and mask layers that recognize the shape of the object. This training approach works in the same way for PROST-Net and Mask R-CNN. A second training phase for fine tuning is made enabling batch normalization in ResNet layers (to prevent overfitting) [26]. This training modifies weights from the 5th stage of ResNet and all the other weights (RPN and head). In this phase, the learning rate (LR) is reduced by a factor 10 from the previous training. The training time of PROST-Net was less than 2 hours on a commercial laptop with an Nvidia RTX 2060m GPU.

PROST-Net's accuracy (computed as Dice score) was 89% on phantom images and allowed segmenting the prostate regardless of the scanning plane (axial or sagittal) and regardless of sensor arrangement (linear or convex) in the case of US images. In patient US images the segmentation accuracy was around 86%; PROST-Net outperformed Mask R-CNN in our application (Fig. 6).

Finally, we tested PROST-Net on MRI images of patients. The training was performed on images taken from the Cancer Imaging Archive [27]. This dataset contains more than 1000 patients and for each entry the prostate gland segmentation and the segmentation of tumours is given. PROST-Net reached a Dice score of 77% on these data (Fig. 5).

The segmentation model was then tested on data obtained from local hospitals under the approved ethical protocol
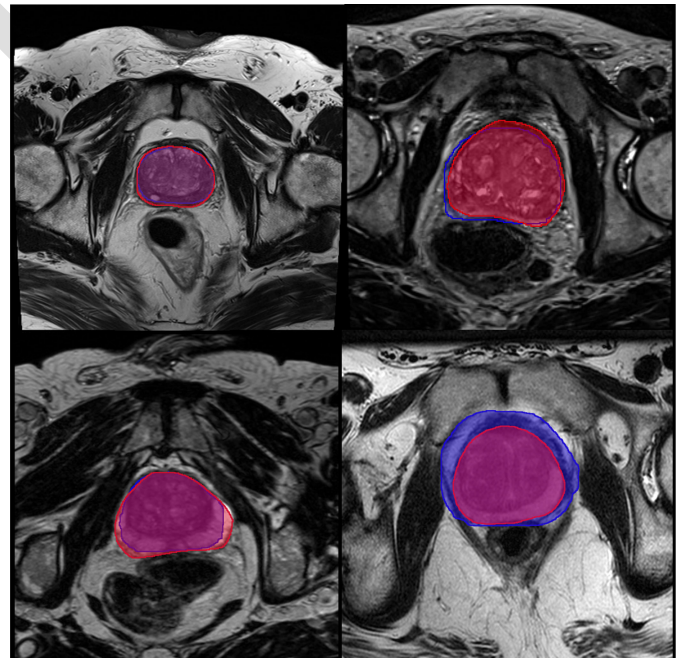
Fig. 5. MRI segmentation of the prostate. Images are taken from different patients. PROST-Net results are in blue; the ground-truth is in red.

3167CESC. Results were similar to those obtained on the publicly available data.

The segmentation of the prostate in MRI allows the initial fusion with a 3D reconstructed and segmented US image acquired with PROST. The segmentation of the lesion in MRI gives to the robot the coordinates of the target. We aim to create a deep learning algorithm for prostate segmentation which is general enough to be used in any clinical case, so that its
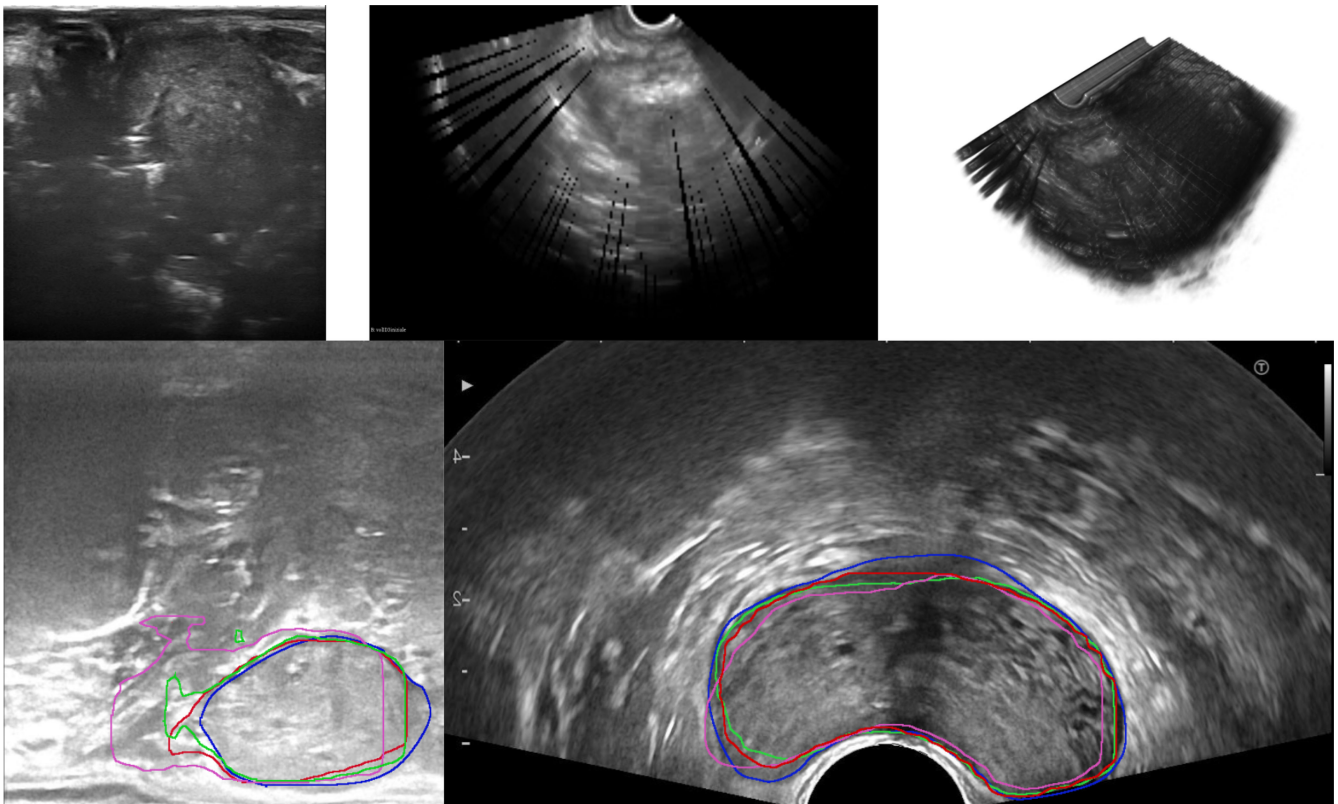
Fig. 6.   **Top Row: ex-vivo images**. Left to right: sagittal US view of a specimen's prostate; axial view of a 3D US reconstruction of a specimen's prostate; volume rendering of a reconstructed prostate. **Bottom Row: in-vivo images**. Axial (left) and sagittal (right) US images of the prostate and segmentation contours. The blue line shows the ground truth. The other lines show the result of the automatic segmentation performed with PROST-Net (Red), Mask R-CNN with ResNet50 (Green) and Mask R-CNN with ResNet101 (Pink). The study was carried out in accordance with ethical approval 3167CESC.

application is feasible in hospitals for MRI-US guided prostate procedures.

IV. MATERIALS AND METHODS

The goal of cadaver testing was to measure PROST's accuracy in targeting points acquired though the imaging of a realistic anatomical space. These target points do not necessarily correspond to lesions in the prostate, which in a clinical setting are the points of greatest interest. Rather than simulating a biopsy by acquiring tissue samples from a previously marked area, material was instead *deposited* in the organ to mark both the target and the position reached by PROST.

The metallic seeds used as markers were of different materials (at first gold, then aluminum and copper), in the same size as those used for brachytherapy, which are typically 3 mm long. The seeds are visible under computed tomography (CT) imaging as multiple punctate metallic attenuation foci, very bright dots with a surrounding starburst pattern. Under ultrasound imaging, on the other hand, seeds are more difficult to discern due to their small size, acoustic artifacts (e.g., seed specularity) and shadowing. Other highly reflective elements in the anatomical surroundings (e.g., calcifications) can also act as decoys and make seed identification difficult.

Five board-certified practicing urologists with relevant clinical experience in prostate interventions (a Full Professor with 25 years of clinical experience, a Researcher with 8 years of clincal experience, and three Residents with 5, 3 and 2 years of clinical experience respectively) participated in this study. Each of the urologists performed different tasks and assisted the tasks carried out by the others. Tasks ranged from preparation and examination of the specimens to needle insertions and prostatectomy. Needle insertions were performed by only one urologist, who was previously trained to use the robot with a preparatory course and has a multi-year experience in transperineal ultrasound-guided prostate biopsies (more than 1200 procedures).

Available cadaver specimens (pelvis to toe tip) were examined via trans-rectal pelvic ultrasound one day in advance of the experiments by an expert urologist. Trans-abdominal ultrasound was available as a back-up, and was used for confirmation in two cases, together with a digital rectal examination, after incurring in a visibility problem with the transrectal probe. Exclusion criteria were the absence of a complete and identifiable prostate and the presence of indicators of prior surgery (e.g., transurethral prostate resection) in the prostate area. To enhance visibility during specimen selection, in one case, a catheter was inserted and the bladder filled with water. Prostatectomy took place after the experiments with PROST. The organ was later dissected by an experienced pathologist.

Due to limited specimen availability and schedule constraints, a total of 10 cadaver specimens were prepared. The initial idea was to place 6 seeds and to target each of them once, so that for each prostate 12 needle insertions would be performed. This scheme would lead to a total number of 120 insertions. Tests were divided in three sets—with 2, 5 and 3
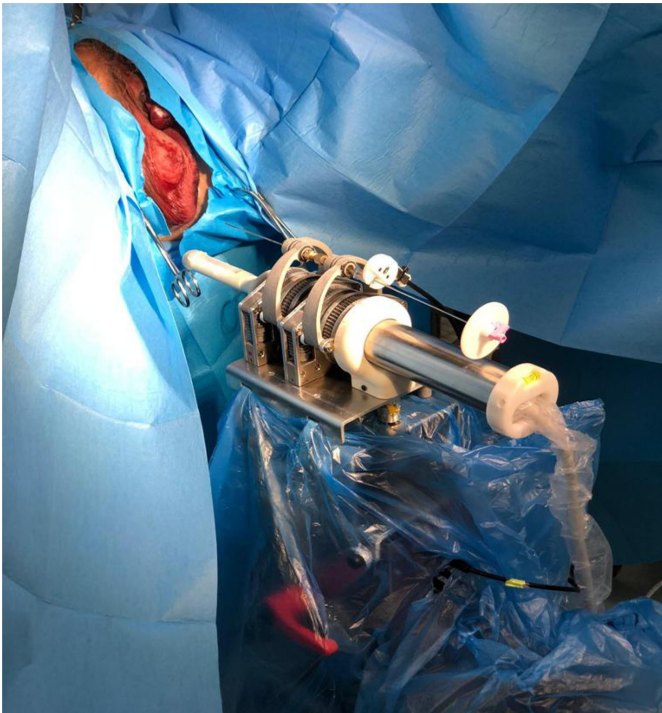
Fig. 7. PROST's positioning robot, prepared for the experiments and shown next to a cadaver specimen in gynecological position.

specimens, respectively. The sets were sufficiently far apart in time that it was possible to analyze the data and hone the experimental procedure, adapting it to the conditions "on the ground."

Whereas the primary objective of the tests was to assess PROST's positioning accuracy in a realistic scenario, a second objective was to determine applicable cross-validation methods for testing prostate procedures on cadavers. The intention was to lay the foundation for pre-clinical validation of other prostate-related procedures (such as brachytheraphy) supported by future PROST prototypes.

All cadavers were placed in the lithotomy position (Fig. 7). For each cadaver, 12 sterile placement needles were prepared, to insert 6 target seeds and 6 reference seeds. The targets marked the position to be reached by the PROST system. The reference seeds were released when the physician performed needle insertion through a guide oriented by PROST. The procedure started with the calibration of the robot and with the US probe positioning in the rectum of the cadaver, so that the prostate is visible in the sagittal plane. For each cadaver, data was collected with the following procedure:

a) Place target seeds into the prostate;
b) Rotate the US probe around its axis so that the next target seed is visible in the 2D US sagittal image;
c) Using PROST's interface, select the location of the target in the US image, and send its coordinates to the positioning robot. Record location as `Target`;
d) PROST autonomously calculates the entry point and orients the cannula toward the target;
e) Manually insert the needle through the cannula, using PROST's GUI to monitor the depth reached by the needle tip. Stop when the circle in the GUI becomes green (the coordinates have been reached). Record the position of the needle tip in robot coordinates and the position within the US image as `RobotTip`, `USTip`;
f) Deposit the reference seed and extract the needle.
g) Return to step (b) until there are no more reachable targets visible in the US and all the reference seeds have been placed;
h) Perform a panoramic US scan and obtain a 3D US reconstruction of the prostate with both target and reference seeds. Record the image as `FinalUSVolume`;

After recording the volume, the physicians performed a prostatectomy for a further histological examination. Before the histological examination, the prostate was imaged under CT and the image was recorded as `CTVolume`.

Note that the seeds are deposited *after* the measurement in step (e). This is to evaluate PROST's ability to reach a target location independently of the later movement of the seeds. A similar approach, that aimed to distinguish between targeting error and biopsy error in robotic prostate biopsy, was introduced in [28], although the indicators used are different. The positioning accuracy thus obtained is the measure of interest for biopsies and the estimate that can be compared with that obtained in prior experiments on phantoms. The relative position of the target and reference seeds, on the other hand, allows evaluating an "anatomical" distance, suited for other prostate-related procedures such as brachytherapy.

Seeds can move significantly in response to different types of events, such as retraction of the biopsy needle, reactive deformation of the prostate due to forces exerted on other parts of the organ, and postural change. The idea was to evaluate the distance between pairs of seeds at different times and in multiple ways:

α directly during the procedure, by leveraging ultrasound imaging and robot kinematics;
β after the procedure, by analyzing the CT scan; and
γ after the removal of the prostate, via histological examination.

Through the process of comparative evaluation, one can contextually acquire a sense of which measures are in agreement with each other and therefore which measures can soundly be used for cross-validation purposes.

The data acquired in phase α in the US reference system and in the robot reference system (`RobotTip`, `USTip`) allow estimating PROST's positioning accuracy; analysis of the CT scan `CTVolume` offers an estimate of the distances between seed pairs that is independent of the robotic system; registering the CT scan from phase β to the 3D US data from phase α (`USTarget`, `USReference`, `FinalUSVolume`) allows comparing seed visibility across imaging modalities, in addition to evaluating seed movement. Lastly, the histological examination provides an assessment of distances between seed pairs that is independent of both imaging and robot.

A. First Set of Experiments (December 2020)

Six pre-loaded sterile placement needles of 18GA diameter and 12 cm length and 6 standard biopsy needles UniGun

(Medax, Modena, Italy) of 18GA diameter and 25 cm length, with the needle core removed, were prepared for each of the 2 cadavers. The biopsy needles are echogenic for ultrasound guided procedures and have a bevel shape tip. By removing the needle core, the stiffness of the needle is reduced, thus making targeted insertion more difficult as compared with biopsy sampling. The bevel tip influences the trajectory by bending the needle in the direction opposite to the bevel. In this set of experiments, seeds were 0.8x3 mm (diameter and length) soft tissue gold markers from CIVCO Radiotherapy (Orange City, IA, USA). The 6 reference seeds were colored with indelible ink before being placed into the biopsy needles, to allow the pathologist to distinguish them from the target seeds during the histological examination. Target and reference seeds are identical under US and CT imaging.

In step (a) target markers were inserted in the prostate by a physician using free-hand technique and relying only on US guidance, as in most traditional prostate biopsies. The intention was to distribute the targets throughout the prostate (2 in the apex, 2 in the midgland, and 2 in the base), to minimize visibility issues due to overlap and facilitate pairing up targets and references.

A major difficulty encountered during the experiments was the seed movement along the needle trail, especially at the time of needle extraction. The experienced urologist anticipated a displacement of approximately 1 cm behind the needle, which also occurs in-vivo, and thus deposited the reference seeds deeper in the tissues then the position recorded in step (e). Although the presence of this phenomenon was known from the experience of the urologist and from literature on brachitherapy [29] and thus foreseeable, its extent was larger than in in-vivo prostate tissue. During the cadaver tests, the movement in the US was 2-3 cm —and on occasion even larger. As a result, some seeds moved outside the prostate and some of the target seeds finished very close to each other in the apex zone. Reference seeds were placed for all target seeds that remained in a reachable location in the prostate.

Another problem had to do with discerning seeds in the anatomical environment due to the presence of calicifications, since the seeds and the calcifications have similar appearance in US imaging.

To address the issues connected with seed visibility and placement, seeds of different lengths and diameters were examined afterwards in the laboratory under US and CT imaging, using phantoms. These seeds were obtained by cutting metal wire. Seeds with 1 mm diameter are significantly easier to discern and track under US imaging then those used in the first set of experiments. Longer seeds also had appreciably lower mobility after insertion in phantoms. Seeds of 4 mm length and 1 mm diameter offered the best compromise between visibility and precision. To accommodate the new seed size, only 25 cm biopsy needles with the core removed were used in later experiments.

B. Second Set of Experiments (February 2021)

In this set of experiments, 1.0x4 mm metallic seeds were prepared by cutting metal wire. The 6 target seeds were in copper and the 6 reference seeds in aluminium. Target and reference seeds are identical under US and CT imaging.

Adjustments in the methodology reflected the experience from the first set of experiments. Differently from before, in step (a) target markers were placed throughout the prostate using PROST. Delivering targets with the robot greatly improves the chance that the seeds will remain within the prostate and in a position reachable by PROST. Insertions were six per cadaver, carried out one target/reference pair at a time, to facilitate measurements and avoid possible confusion with other target/reference pairs. One additional data-collection step was added to the experimental procedure after step (f):

$\bar{f}_2$ Move the US probe to bring the target seed in view and acquire its position in the US image. If necessary, move the probe again to see the reference seed and then acquire the US coordinates. Record the values as USTarget, USReference.

Due to a combination of favorable factors (seeds were larger, more visible and the physician was more familiar with how much they move along the needle trail in cadavers), more care was paid to step (f). Once the seed started moving behind the needle, the physician used the needle to give a gentle tap to the seed, which often would result in the seed changing orientation and being gripped by the surrounding prostatic tissue. As a result, most seeds remained within the prostate, more closely following the intended positioning scheme (2 each in the apex, midgland, base).

In three cases, however, the histology results returned a lower number of seeds than were inserted in the prostate. The working hypothesis is that the seeds may have moved to or past the prostatic capsule, and that they were not collected with the rest of the gland during prostatectomy. The seeds had good visibility in the images FinalUSVolume and CTVolume; seeds were also easier to distinguish from calcifications. Even though the exact confines of the prostate are not easily discernible in CT imaging, we decided after this experiment to perform a CT scan prior to prostatectomy.

A point-based algorithm [30] was used to rigidly register USTarget and USReference to CTVolume. The very large error in the results made an irrefutable matching impossible. The correspondence between imaging modalities was lost when the urologist would reposition the ultrasound probe (and thus also the base of the robot to which is joined), to restore lost contact between the probe and the rectum. Unfortunately, the movement of the base was unplanned and therefore not encoded in the robot kinematics. As a result, because the window of best visibility of the robot was brought to overlap different areas of the prostate, the points described by USTarget and USReference appeared much closer together than in FinalUSVolume or CTVolume.

C. Third Set of Experiments (April 2021)

In this set of experiments, each of the 3 cadaver specimens was imaged under CT *before* prostatectomy took place.

Histological examination determined that the sample previously extracted from specimen with ID 5, believed to be an intact prostate, was in fact composed of adipose and muscle
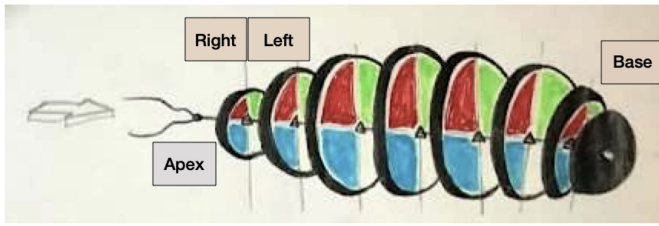
Fig. 8. Macrosections for histological examination of the prostate. Each 5mm-thick slice is divided in quadrants, to mark the right/left and superior/inferior regions.

₆₃₀ tissue only. The insertion of the seeds and the targeting in this ₆₃₁ tissue gave similar results to the other experiments (Table I). ₆₃₂ After determination that it did not have a prostate, specimen ₆₃₃ with ID 10 was retained to serve as a further experimental ₆₃₄ control for the general pelvic area.

D. Histological Examination

₆₃₆ Samples from radical prostatectomy were fixed in 10% ₆₃₇ buffered formalin, with surgical thread marking the apex. After ₆₃₈ fixation, specimens were sectioned at 5 mm intervals following ₆₃₉ the axis of the prostatic urethra (Fig. 8). Samples were col- ₆₄₀ lected together with their surrounding fat tissues, in an effort to ₆₄₁ preserve seeds that may have moved past the boundaries of the ₆₄₂ organ. One of the samples was found to be composed entirely ₆₄₃ of adipose and muscle tissue, and not to contain prostatic ₆₄₄ parenchyma.

₆₄₅ All sections were visually examined and palpated to locate ₆₄₆ the seeds. Distances were measured from the reference planes ₆₄₇ A (apex), B (base), DX (right) and SN (left). Colored ink was ₆₄₈ injected into the space occupied by the seeds and the small ₆₄₉ round holes clearly originated by a needle.

₆₅₀ Macrosections were further processed into 4 μm slices; one ₆₅₁ microsection every 500 μm was retained and stained with ₆₅₂ hematoxylin and eosin. Distances from the reference planes ₆₅₃ were recalculated for confirmation whenever seeds were found ₆₅₄ in the stained microsections.

V. RESULTS AND DISCUSSION

₆₅₆ Accuracy measured through the phantom tests accounts for ₆₅₇ the errors introduced by the calibration and mechanical oper- ₆₅₈ ation of PROST and by needle tip deflection. In phantoms, ₆₅₉ deflection is mostly a function of distance travelled inside ₆₆₀ the phantom. Cadaver experiments refine this measure by also ₆₆₁ including a critical and hard-to-estimate component of local- ₆₆₂ ization error: the extent to which the biopsy needle deflects as ₆₆₃ it travels through inhomogeneous materials of variable stiff- ₆₆₄ ness and compressibility — the human tissues in the pelvic ₆₆₅ area. This measure is of key importance. In the absence of a ₆₆₆ predictive model that could be used by the PROST software to ₆₆₇ compensate for the needle deflection when calculating access ₆₆₈ paths for the biopsy, this error component cannot be reduced ₆₆₉ without great effort and without incurring much higher costs.

₆₇₀ Table I reports the experimental values for positioning error ₆₇₁ (mean μ and standard deviation σ), calculated as the distance

TABLE I
NUMERICAL RESULTS. COLUMNS REPRESENT EXPERIMENT NUMBER (SET), SPECIMEN NUMBER (ID), NUMBER OF SEEDS TARGETED (SAMPLES), AND THE DISTANCE BETWEEN THE NEEDLE TIP AND THE SEED IN THE ROBOTIC REFERENCE SYSTEM (ROBOTTIP AND USTIP) AND IN THE US REFERENCE FRAME (LAST COLUMN)

| Set | ID | Samples | Needle tip−Target | | | | USReference−USTarget | |
| | | | RobotTip | | USTip | | US | |
			μ	σ	μ	σ	μ	σ
1st	1	3	2.29	0.67	2.88	0.92	5.20	2.74
2nd	3	4	2.15	0.78	2.47	1.05	4.71	2.66
	4	6	1.81	1.21	2.10	1.01	3.40	1.07
	5	6	2.02	0.55	2.44	1.17	3.12	1.09
	6	6	1.94	0.82	2.49	0.45	3.07	0.51
	7	6	1.55	0.34	1.82	0.62	2.58	0.82
3rd	8	6	3.37	0.31	1.97	0.69	2.89	0.39
	9	6	1.63	0.58	1.94	0.31	2.15	0.44
	10	6	2.07	0.86	2.37	0.50	2.24	0.98
Overall (prostate only)			2.09	0.66	2.17	0.69	3.22	1.03
Overall (all tests)			2.08	0.67	2.23	0.72	3.08	1.03

₆₇₂ between a target location and the position reached by the nee- ₆₇₃ dle tip. The coordinates of the target location (target seed) are ₆₇₄ taken from the US image, mapped into the robot reference ₆₇₅ system. This signal was recorded as Target. The position of ₆₇₆ the needle tip is calculated in two ways, to yield the values ₆₇₇ in the columns labeled RobotTip and USTip. The posi- ₆₇₈ tion recorded as RobotTip is given by the robot kinematics ₆₇₉ and the TOF sensor, whereas USTip records the coordinates ₆₈₀ in the US image through the reference system of the PROST ₆₈₁ robot. Positioning data for cadaver No.2 was lost, due to equip- ₆₈₂ ment malfunction and loss of calibration with the US probe ₆₈₃ software.

₆₈₄ The difference between the two error estimates is in large ₆₈₅ part due to the deflection of the needle —in turn due to the ₆₈₆ bevel tip and its small diameter— and can be used to estimate ₆₈₇ it. Beside the case with ID 8, the results are homogeneous and ₆₈₈ the maximum contribution of the needle deflection is in the ₆₈₉ range $0.29 - 0.59$ mm, with an average of 0.38 ± 0.12 mm. ₆₉₀ The analysis of the CT scan of specimen with ID 8 showed ₆₉₁ a heavy extent of calcifications in the prostate gland and we ₆₉₂ strongly believe that this affected the trajectory of the needle ₆₉₃ and eventually caused movement of the target seeds.

₆₉₄ We find that in a realistic anatomical environment the nee- ₆₉₅ dle deflection contributes as little as 0.5 mm to the overall ₆₉₆ positioning error. We believe that this number can be con- ₆₉₇ sidered a meaningful first estimate for the impact of needle ₆₉₈ deflection on the accuracy of the PROST positioning robot ₆₉₉ when targeting the prostate in anatomical environments. This ₇₀₀ measure is obtained when sampling both anterior and poste- ₇₀₁ rior positions in the prostate, as confirmed by the histology: ₇₀₂ seeds were found in both peripheral and internal/central areas ₇₀₃ (Column P and C in Table II).

₇₀₄ In most of the tests, the tip of the needle and the center ₇₀₅ of the target seed are in the same US plane; as a result, the
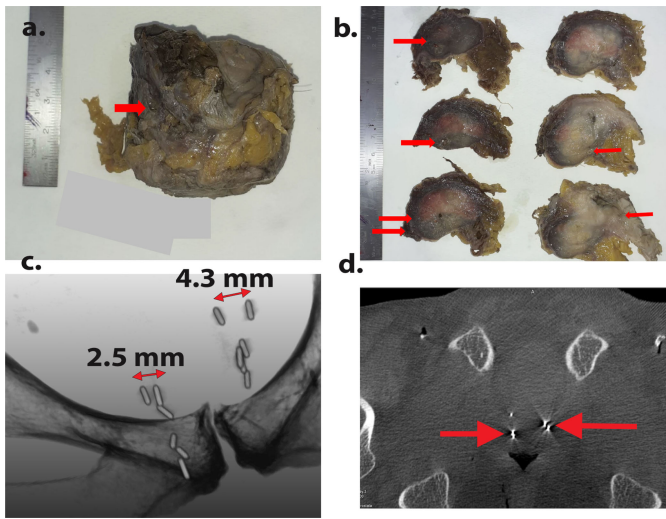
Fig. 9. **a.** Specimen's prostate after removal. **b.** Macro-slices with arrows pointing to seeds. **c.** 3D volume rendering of a CT scan, prior to prostatectomy. All 12 seeds are visible. The identity of matching seeds can be inferred and the distance computed, but without certainty of correct pairing, since the seeds are identical in the image. **d.** CT scan slice. The seeds are reflective and easily identified, but the contour of the prostate is hardly visible.

TABLE II

SUMMARY OF CASES. COLUMNS REPRESENT SPECIMEN NUMBER (ID), NUMBER OF TARGET SEEDS INSERTED (TIn), NUMBER OF REFERENCE SEEDS INSERTED (RIn), TOTAL NUMBER OF SEEDS INSERTED (In), NUMBER OF SEEDS VISIBLE IN THE CT SCAN OF THE PROSTATE (CT), NUMBER OF SEEDS FOUND DURING HISTOLOGICAL EXAMINATION (H), PRESENCE OF SEEDS IN THE EXTERNAL/PERIPHERAL HALF OF THE PROSTATE (P) AND IN THE INTERNAL/CENTRAL HALF (C), LENGTH OF THE PROSTATE ALONG THE APEX-BASE AXIS IN CM (AB), AND NUMBER OF PAIRS MEASURED IN THE US IMAGE (USP), IN PARTICULAR DURING STEP ($\bar{h}_2$). WHEN TARGET SEEDS MIGRATED OUTSIDE THE PROSTATE OR HAD BECOME UNREACHABLE, RIn IS LESS THAN TIn (IN ORANGE). SHOWN IN BLUE ARE THE CASES WHEN INSERTED SEEDS WERE NOT ALL FOUND IN THE CT VOLUME, OR SEEDS COUNTED IN CT WERE NOT FOUND IN HISTOLOGY. THE USP PAIRS WERE USED TO CALCULATE THE VALUES USReference–USTarget IN TABLE I

Set	ID	TIn	RIn	In	CT	H	P	C	AB	USP
1st	1	6	3	9	–	9	✓	✗	6.4	3/3
	2	6	4	10	–	10	✓	✓	7.0	0
2nd	3_1	6	4	10	10	9	✓	✓	6.8	4/4
	4_2	6	6	12	11	11	✗	✓	6.3	6/6
	5_3	6	6	12	5	◆	◆	◆	∼ 4	6/6
	6_4	6	6	12	8	0	✗	✗	N/A	6/6
	7_5	6	6	12	11	7	✗	✓	7.1	6/6
3rd	8_1	6	6	12	12	7	✓	✓	6.0	6/6
	9_2	6	6	12	12	7	✓	✓	6.3	6/6
	10	6	6	12	12	◆	◆	◆	◆	6/6

USTip error is calculated independently of the robot kinematics. When the two elements were not in the same US plane, the probe was slightly rotated to acquire the two positions. In this second situation, the measurement is not independent of the robot kinematics; however, considering that the rotation required is small and that it was required in few cases, the measure is likely to be only marginally affected by the robot kinematics. In the context of biopsy procedures, USTip error is the more meaningful measure of PROST's positioning accuracy.

A limitation of this study is the relatively small number of data points—an almost inevitable factor when experimenting on cadavers. However, the data is sufficient and sufficiently homogeneous to indicate a reliable range.

In spite of the shortcomings of cadaveric tests, most measurements fall within the desired accuracy for needle biopsy, with an overall mean of 2.25 mm and a standard deviation of 0.75 mm. Suitability for clinical practice derives from being able to reliably biopsy any lesion of clinical significance, typically larger than 5-7 mm. These are very encouraging results considering the difficulties described above.

A second line of investigation concerned cross-validation methods, comparing information offered about the location of seeds by different imaging modalities (Fig. 9 and 10). Data collected allowed estimating the degree to which seeds akin to those used in brachytherapy move within the prostate in response to forces exerted by needle retraction, additional puncturing of the prostate, prostatectomy and preparation for histological examination.

Table II reports an overview of the experiments. The measurement technique used is the same as for USTip. However, this time most tests required rotating the US probe, so the measurement cannot be treated as independent of the kinematics. The seed-to-seed distance exceeds the needle-to-seed distance by more than 2mm in the first set of experiments and reduces progressively, down to less than 0.5 mm for the last set, indicating that the countermeasures described in Section IV-B were very successful. Movement during needle retraction may include rotation, in addition to the preferential motion along the needle track. After needle retraction, pairs of seeds lie at an average distance of 3mm (range 1-6 mm).

The movement of the US probe in the transperineal approach implemented by PROST is a rotation around its axis, thus minimizing the deformation of the prostate as compared with the transrectal approach that involves an end-fire US probe which rotates around a fulcrum [31]. Nevertheless, cadaver tissues have undergone significant deformation. The lack of vascularization in the cadaveric prostate is very impactful, making the prostate far less elastic than a normal in-vivo sample of similar stiffness. Needle insertions and retractions created large tissue displacements that were semi-permanent and displaced most of the seeds already inserted—with some seeds observed to be moving along the needle trails. The needle trails were at times visible for the whole duration of the experiment and even masked the seed positions in the US images.

The data collected had a measure of redundancy– to improve robustness in the estimates and to limit the risk of the experiments not yielding useful data. Multiple independent data streams can also lessen the dependence of the measures on the PROST system. Not all data collected for cross-analysis were useful, because of the peculiar nature of ex-vivo prostate tissues and the difficulty in matching sets of moving elements with only partial data available (missing seeds).
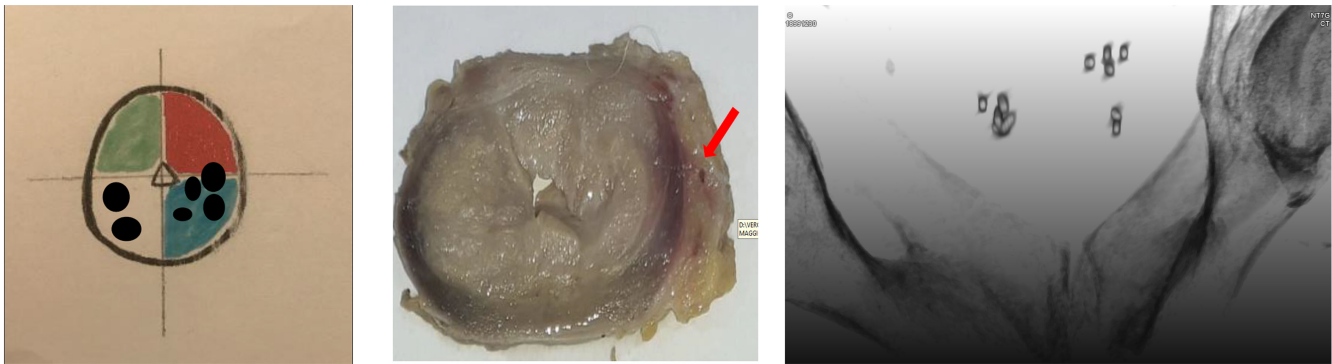
Fig. 10. **Left:** Drawing of the seeds (in black) projected into a slice divided in quadrants. **Center:** A macro-slice of the same prostate with one seed identified (red arrow). **Right:** CT 3D rendering of the same specimen with the disposition of all the seeds before prostatectomy.

CT scans obtained in the third set of experiments (e.g., Fig. 9c) show seed configuration after the prostate underwent 12 punctures. The signatures of target and reference seeds in CT were too similar to distinguish, requiring the assistance of histology. The images allowed estimating the distance between pairs of seeds, but without being able to assess which seeds were part of which pairs. The 3D US images `FinalUSVolume` were not by themselves able to provide confirmation and circumvent the issue of missing seeds in CT, because the visibility of the seeds was affected by the calcifications present in most of the cadaveric prostates, and it was difficult to identify all 12 seeds with confidence.

CT scans obtained in the second set of experiments showed the seed configuration after the additional stresses of prostatectomy. Removing the prostate from its site deformed the organ and caused the seeds to move, to such an extent that the seed-to-seed correspondence was potentially lost. Seeds were lost in the process, especially from the outer area.

An additional loss of markers is due to machine processing for histology. Samples are dehydrated, heated, and subjected to a number of mechanical stresses. In case with ID 6, *all* seeds were lost, an indication that integrating histology into these investigations will require careful adjustments.

Colored seeds are distinguishable in the histological images (Fig. 9b); however, due to the large deformations and seed movements and to the loss of seeds, in most cases it was not possible to assume that a seed's closest neighbor is its match in a target/reference pair.

VI. CONCLUSION AND FUTURE WORK

The primary goal of cadaver experiments was to assess PROST's positioning accuracy in a realistic anatomical environment. The experiments place the accuracy at 2.25 ± 0.75 mm, a performance level compatible with clinical requirements and obtained in the more challenging arena of post-mortem in situ testing. Results also allow estimating the component of the error due to needle deflection as 0.38 ± 0.12 mm.

Further pre-clinical validation of the segmentation module is ongoing on patient data. These tests are in a preliminary phase and we are extending the training of the segmentation algorithm —PROST-Net— with MRI and US data coming from 7 hospitals in Italy, including at least 200 patients for each center. These additional data will allow improving our current estimates. Another line of research is tumour identification in multiparametric MR to increase the autonomy of PROST in detecting the cancer suspect region and in automatic definition of a suitable trajectory. In fact, the PROST-Net architecture is easily extendable to additional classes of objects such as tumours. The MRI-US contour fusion, will give the initial alignment between the robot and the MR image where the target was defined. Even though PROST's perineal approach limits the extent of prostate deformation, the prostate is still subject to direct forces exerted by the needle or delivery mechanism and to reactive forces from the surrounding tissues. Real-time segmentation of 2D US images enable adapting to the intra-operative deformation and displacement of the prostate, thus preventing the degradation of accuracy.

Increasing the autonomy of the system is helpful because tasks that humans cannot reliably succeed at —due to limitations in precision, accuracy, stamina and speed— become feasible with machine assistance.

To enhance autonomy, PROST will employ machine learning for a variety of cognitive tasks, such as pre-operative image analysis, diagnostics, target selection, fusion of MRI and real-time US images, entry point and trajectory planning–each adding a measure of autonomy to a phase of the procedure.

Cognitive assistance can be expected to grow in importance and sophistication, incorporating progressively more domain knowledge and contextual information. This feature is especially valuable for tasks that require experience and specialized expertise–where the machines can leverage access to case libraries and to statistics from medical literature–and difficult perceptual tasks that are negatively impacted by fatigue, where machines can help by providing consistent and automatic anomaly detection.

A prostate biopsy robot such as PROST has several potential advantages ranging from accurate targeting comparable with MR guided biopsy but with the advantage of real-time US guidance and 3D visualization, standardization of the biopsy procedure regardless of the user's experience level, repeatability of the biopsy for active surveillance to the possibility of combining the robot with other diagnostic and therapeutic device (e.g., *in situ* optical biopsy using optical coherence tomography (OCT), brachytherapy,

microwave ablation, cryoablation). Particular attention will be paid to the sterilization constraints. Small parts in contact with the needle will be removable and disposable; the mechanical part will be detachable from the electronic part for autoclave sterilization.

The direct experience gained in this research affords us an understanding the importance of different features for clinical situation awareness and excellent performance. The team is better positioned to make design and resource allocation decisions, so as to invest first in the improvements that matter most. Some features highlighted during this research are the ability to account for deformations and accurately track seeds, improvements in mechanical accuracy and predictive models, improvements in usability, sterilization, extension of the workspace.

ETHICAL APPROVAL

All procedures performed in this study were in accordance with the ethical standards of the institutional and/or national research committee and with the 1964 Helsinki Declaration and its later amendments or comparable ethical standards (ethical approval number 3167CESC).

REFERENCES

[1] C. H. Pernar, E. M. Ebot, K. M. Wilson, and L. A. Mucci, "The epidemiology of prostate cancer," *Cold Spring Harbor Perspect. Med.*, vol. 8, no. 12, 2018, Art. no. a030361.

[2] N. Mottet *et al.*, "EAU-EANM-ESTRO-ESUR-SIOG guidelines on prostate cancer-2020 update. Part 1: Screening, diagnosis, and local treatment with curative intent," *Eur. Assoc. Urol.*, vol. 79, no. 2, pp. 243–262, 2021.

[3] E. Baco *et al.*, "A randomized controlled trial to assess and compare the outcomes of two-core prostate biopsy guided by fused magnetic resonance and transrectal ultrasound images and traditional 12-core systematic biopsy," *Eur. Urol.*, vol. 69, no. 1, pp. 149–156, 2016.

[4] V. Kasivisvanathan *et al.*, "MRI-targeted or standard biopsy for prostate-cancer diagnosis," *New England J. Med.*, vol. 378, no. 19, pp. 1767–1777, 2018.

[5] A. Leroy, M. Baumann, P. Mozer, J. Troccaz, and V. Daanen, "System and method for imaging and locating punctures under prostatic echography," U.S. Patent 8 369 592, Feb. 5, 2013.

[6] S. Lim, C. Jun, D. Chang, D. Petrisor, M. Han, and D. Stoianovici, "Robotic transrectal ultrasound guided prostate biopsy," *IEEE Trans. Biomed. Eng.*, vol. 66, no. 9, pp. 2527–2537, Sep. 2019.

[7] J. Xiang, H. Yan, J. Li, X. Wang, H. Chen, and X. Zheng, "Transperineal versus transrectal prostate biopsy in the diagnosis of prostate cancer: A systematic review and meta-analysis," *World J. Surg. Oncol.*, vol. 17, no. 1, pp. 1–11, 2019.

[8] J. Grummet, "How to biopsy: Transperineal versus transrectal, saturation versus targeted, what's the evidence?" *Urol. Clin. North Amer.*, vol. 44, no. 4, pp. 525–534, 2017.

[9] W. L. Ong *et al.*, "Transperineal biopsy prostate cancer detection in first biopsy and repeat biopsy after negative transrectal ultrasound-guided biopsy: The victorian transperineal biopsy collaboration experience," *BJU Int.*, vol. 116, no. 4, pp. 568–576, 2015.

[10] V. Stefanova *et al.*, "Transperineal prostate biopsies using local anesthesia: Experience with 1,287 patients. Prostate cancer detection rate, complications and patient tolerability," *J. Urol.*, vol. 201, no. 6, pp. 1121–1126, 2019.

[11] D. Stoianovici *et al.*, "MR safe robot, FDA clearance, safety and feasibility prostate biopsy clinical trial," *IEEE/ASME Trans. Mechatronics*, vol. 22, no. 1, pp. 115–126, Feb. 2017.

[12] D. Stoianovici, L. L. Whitcomb, D. Mazilu, R. H. Taylor, and L. R. Kavoussi, "Remote center of motion robotic system and method," U.S. Patent 7 021 173, Apr. 4, 2006.

[13] F. J. Siepel, B. Maris, M. K. Welleweerd, V. Groenhuis, P. Fiorini, and S. Stramigioli, "Needle and biopsy robots: A review," *Current Robot. Rep.*, vol. 2, pp. 73–84, Jan. 2021.

[14] B. Maris *et al.*, "Toward autonomous robotic prostate biopsy: A pilot study," *Int. J. Comput. Assist. Radiol. Surg.*, vol. 16, no. 8, pp. 1393–1401, 2021.

[15] M. M. Swindle, A. Makin, A. J. Herron, F. J. Clubb Jr., and K. S. Frazier, "Swine as models in biomedical research and toxicology testing," *Vet. Pathol.*, vol. 49, no. 2, pp. 344–356, 2012.

[16] A. Lasso, T. Heffter, A. Rankin, C. Pinter, T. Ungi, and G. Fichtinger, "PLUS: Open-source toolkit for ultrasound-guided intervention systems," *IEEE Trans. Biomed. Eng.*, vol. 61, no. 10, pp. 2527–2537, Oct. 2014.

[17] J. Tokuda *et al.*, "OpenIGTLink: An open network protocol for image-guided therapy environment," *Int. J. Med. Robot. Comput. Assist. Surg.*, vol. 5, no. 4, pp. 423–434, 2009.

[18] G.-Z. Yang *et al.*, "Medical robotics—Regulatory, ethical, and legal considerations for increasing levels of autonomy," *Sci. Robot.*, vol. 2, no. 4, p. 8638, 2017.

[19] T. Haidegger, "Autonomy for surgical robots: Concepts and paradigms," *IEEE Trans. Med. Robot. Bionics*, vol. 1, no. 2, pp. 65–76, May 2019.

[20] L. Palladino, B. Maris, and P. Fiorini, "3D slicer module for semantic segmentation of ultrasound images in prostate biopsy using deep learning techniques," in *Proc. CARS Comput. Assis. Radiol. Surg. 34th Int. Congr. Exhibit.*, 2020.

[21] L. Palladino, B. Maris, A. Antonelli, and P. Fiorini, "Autonomy in robotic prostate biopsy through AI-assisted fusion," in *Proc. IEEE 20th Int. Conf. Adv. Robot. (ICAR)*, 2021, pp. 142–147.

[22] K. He, G. Gkioxari, P. Dollár, and R. Girshick, "Mask R-CNN," in *Proc. IEEE Int. Conf. Comput. Vis.*, 2017, pp. 2961–2969.

[23] O. Ronneberger, P. Fischer, and T. Brox, "U-Net: Convolutional networks for biomedical image segmentation," in *Proc. Int. Conf. Med. Image Comput. Comput.-Assist. Interv.*, 2015, pp. 234–241.

[24] K. He, X. Zhang, S. Ren, and J. Sun, "Deep residual learning for image recognition," in *Proc. IEEE Conf. Comput. Vis. Pattern Recognit.*, 2016, pp. 770–778.

[25] M. A. Morid, A. Borjali, and G. Del Fiol, "A scoping review of transfer learning research on medical image analysis using ImageNet," *Comput. Biol. Med.*, vol. 128, Jan. 2021, Art. no. 104115.

[26] J. Huang *et al.*, "Speed/accuracy trade-offs for modern convolutional object detectors," in *Proc. IEEE Conf. Comput. Vis. Pattern Recognit.*, 2017, pp. 7310–7311.

[27] S. Natarajan, A. Priester, D. Margolis, J. Huang, and L. Marks, 2020, "Prostate MRI and Ultrasound With Pathology and Coordinates of Tracked Biopsy (Prostate-MRI-U.S.-Biopsy)," Wiki. [Online]. Available: https://wiki.cancerimagingarchive.net/x/BQAWB

[28] M. G. Schouten *et al.*, "Evaluation of a robotic technique for transrectal MRI-guided prostate biopsies," *Eur. Radiol.*, vol. 22, no. 2, pp. 476–483, 2012.

[29] J. R. Lobo *et al.*, "Use of needle track detection to quantify the displacement of stranded seeds following prostate brachytherapy," *IEEE Trans. Med. Imag.*, vol. 31, no. 3, pp. 738–748, Mar. 2012.

[30] B. M. Maris and P. Fiorini, "Generalized shapes and point sets correspondence and registration," *J. Math. Imag. Vis.*, vol. 52, no. 2, pp. 218–233, 2015.

[31] M. Baumann, P. Mozer, V. Daanen, and J. Troccaz, "Prostate biopsy tracking with deformation estimation," *Med. Image Anal.*, vol. 16, no. 3, pp. 562–576, 2012.